Investigation of the Impact of Weather on Multi-Machine Transient Stability Analysis

Arif Ahmed*, Fiona Stevens McFadden†, Ramesh Rayudu‡, and Tobias Massier§

*†Robinson Research Institute, *‡Smart Power and Renewable Energy Systems Group

*†‡School of Engineering and Computer Science, Victoria University of Wellington, Wellington 6140, New Zealand

*§TUMCREATE, 1 CREATE Way, #10-02 CREATE Tower, Singapore 138602

Email: *arif.ahmed@tum-create.edu.sg, †fiona.stevensmcfadden@vuw.ac.nz,

‡ramesh.rayudu@vuw.ac.nz, and §tobias.massier@tum-create.edu.sg

Abstract—Transient stability analysis (TSA) deals with insta-bility due to large disturbances in the power system. Tradi-tionally, TSA of multi-machine systems is performed by time-consuming time-domain simulations based on simplified assump-tions that do not model the weather-dependent characteris-tics. However, the weather affects power flow analysis (PFA). Therefore, an impact of weather on TSA is anticipated. In this manuscript, the weather-dependent impacts are fully modelled and considered for TSA of multi-machine systems. Consequently, the impacts of weather on the transient stability of a multi-machine system is investigated by considering real weather data. The influence of weather on TSA of transmission and distribution networks by performing time-domain fault simulations are car-ried out to demonstrate clearly that varying weather conditions impact the machine rotor angles and critical fault clearing times, causing these to vary with the weather, unlike conventional multi-machine transient stability analysis (MMTSA). It is also demonstrated that consideration of weather for TSA is more suitable for distribution networks having high R/X ratios and lower inertia.

Index Terms—Transient Stability Analysis, Weather Depen-dent Transient Stability Analysis, Multi-machine Systems

I. INTRODUCTION

Transient stability analysis (TSA) is an essential part of power system stability (PSS), that involves study of the power system following a large/major disturbance (faults, loss of generation, line outage, etc.) [1]–[4]. The acceleration of the rotor shaft of a synchronous generator varies during a large disturbance, the dynamics of which are described by the swing equation [1]–[4]. The return of the rotor to a stable steady-state condition following the clearance of a large disturbance is ascertained by TSA.

A substantial effort has been spent in the field of PSS to make TSA of power systems more accurate, reliable, and computationally efficient in order to analyse the stability of power networks [5], [6]. However, despite the progress made, major blackouts have still occurred in the last decade [5], [7], and the stability of modern power systems is constantly being threatened as they are increasingly being operated closer to their stable limits. Furthermore, modern power networks having bi-directional power flow capabilities, distributed gen-eration, communication infrastructure, etc. are also threatening the stability of power systems. In addition, there is a rising concern of climate change worldwide [8], and its impact on

the PSS is not known. The impact of weather on power system analysis has been recently modelled and studied [9], [10] but its impact on PSS of multi-machine systems has not been investigated. Stability analysis incorporating a range of realistic factors, such as weather parameters, is still essential for accurate modelling and studying of PSS, which will aid in stable and secure operation of the power network.

Traditionally, TSA of multi-machine systems is performed via time-domain simulations by solving differential-algebraic equations (DAE) [1]–[4]. The traditional approach is based on simplified assumptions and the weather-dependent character-istics are not modelled. It is demonstrated that the weather affects power flow analysis (PFA) [9], [10] and incorporating weather-dependent characteristics improves the accuracy of PFA [9], [10]. Consequently, the incorporation of weather into TSA of multi-machine systems is expected to improve the analysis (as demonstrated in the single-machine infinite-bus system (SMIB) [11]–[13]).

A handful of studies to improve TSA of SMIB by consider-ing weather or weather-dependent effects can be found in the literature. A temperature-dependent transmission line model was proposed in [11], which was then utilised to highlight the potential impact of conductor temperature on the transient stability of an SMIB system. Instead of using a heat balance model to obtain accurate weather-dependent conductor tem-perature, the authors in [11] assumed a predefined conductor temperature (for demonstration) that depends on the weather condition. Difference in the stability indicators, i.e. critical clearing angle and time of the SMIB were observed in [11], which demonstrated the significance of considering weather information for accurate TSA. However, the assumption of predefined conductor temperatures and neglecting the use of a heat balance model for conductors does not yield accurate impact of weather on conductor temperature and hence in TSA. As a result, a first attempt to incorporate weather param-eters into TSA of an SMIB system was undertaken in [12] by utilizing a linear thermal resistance model [14]. In comparison to the conventional approach, changes in the power-angle curve and stability indicators were observed in [12], which varied with the length and type of conductors indicating the importance of accurate modelling by consideration of the impact of weather in PSS studies. More recently, the steady-

state nonlinear heat balance model (based on the IEEE 738[TM]-2012 [15]) of a conductor was utilized to fully and accurately incorporate the effect of weather in the study of TSA of an SMIB system. These aforementioned investigations reveal that accounting for the weather or weather-dependent effects aid in a more accurate analysis as compared to the conventional approach.

A study of the impact of weather conditions on TSA of multi-machine systems is not present in the extant literature. Consequently, it not clear how significantly and to what extent weather could impact TSA of multi-machine systems. Therefore, in this manuscript, a methodology to perform weather-dependent MMTSA is presented and utilised to investigate the impact of weather on the transient stability of multi-machine systems via a simulation case study. For the simulation case study, the IEEE 30-bus system is modified to represent both the transmission and distribution network, and MMTSA is investigated using real weather data. This manuscript addresses the gap of understanding the impact of weather on TSA of multi-machine systems.

Section II of the manuscript presents an overview of the weather-dependent power flow (WDPF) algorithm, Section III discusses the weather-dependent MMTSA approach, followed by Section IV which presents the simulation case study details. Simulation results are presented and discussed in Section V. The manuscript is concluded in Section VI.

II. Overview of Weather-Dependent Power Flow

Recently, the weather-dependent power flow algorithm (WDPF) [10] which fully incorporates the nonlinear effects of weather to perform an accurate PFA was presented. The WDPF algorithm is explicitly parameterised in terms of commonly available and measured weather parameters, and uses the steady-state nonlinear heat balance model of overhead conductors presented in the IEEE Std 738[TM]-2012 [15].

The steady-state nonlinear heat balance model is given in Equation (1). Details can be found in [10], [15].

$$q_c + q_r = q_s + q_j \qquad (1)$$

In Equation (1), q_c is the convective cooling rate, q_r is the radiative cooling rate, q_s is the solar heat gain rate, and q_j is the Joule heat gain rate or the heat gain rate due to resistive losses (all in W/m).

The nonlinear heat balance Equation (1) can be solved to calculate the conductor temperature ($T_{c_{ij}}$) given the weather conditions, conductor characteristics, and line loading. Under steady-state condition, the nonlinear heat balance Equation (1) for a conductor between Bus i and Bus j, can be represented as a function of conductor temperature as shown in Equation (2) [10]. In Equation (2), E and F are the real part and the imaginary part of the complex voltage (pu) in rectangular form. g_{ij} is the branch conductance (in pu).

Based on Equation (2), a mismatch equation of the steady-state nonlinear heat balance is formed to calculate the conductor temperature ($T_{c_{ij}}$) as represented in Equation (3).

$$\Delta H_{ij} = -H_{ij}^{calc} \qquad (3)$$

In Equation (3), H_{ij}^{calc} is the calculated value of the nonlinear heat balance function.

Equation (2) is essential to deriving the WDPF algorithm. The heat balance mismatch vector is formed for all the weather-dependent branches in a network and then appended to the conventional power flow algorithm (PF) [1], [2], [16] (in rectangular formulation) to derive the update equation of the WDPF algorithm as:

$$\begin{bmatrix} \boldsymbol{E} \\ \boldsymbol{F} \\ \boldsymbol{T_c} \end{bmatrix}^{(v+1)} = \begin{bmatrix} \boldsymbol{E} \\ \boldsymbol{F} \\ \boldsymbol{T_c} \end{bmatrix}^{(v)} + \boldsymbol{J}^{-1(v)} \begin{bmatrix} \boldsymbol{\Delta P} \\ \boldsymbol{\Delta Q} \\ \boldsymbol{\Delta V^2} \\ \boldsymbol{\Delta H} \end{bmatrix}^{(v)} \qquad (4)$$

In Equation (4), v is the iteration number, $\boldsymbol{E}$ is the vector of voltages (real part), $\boldsymbol{F}$ is the vector of voltages (imaginary part), $\boldsymbol{T_c}$ is the vector of weather-dependent branch temperatures, $\boldsymbol{\Delta P}$ is the vector of real power mismatch, $\boldsymbol{\Delta Q}$ is the vector of reactive power mismatch, $\boldsymbol{\Delta V^2}$ is the vector of bus voltage magnitude-squared mismatch, and $\boldsymbol{\Delta H}$ is the heat balance mismatch vector. $\boldsymbol{J}$ in Equation (5) is defined as:

$$\boldsymbol{J}_{\text{new}} = \begin{bmatrix} \frac{\partial \boldsymbol{P}}{\partial \boldsymbol{E}} & \frac{\partial \boldsymbol{P}}{\partial \boldsymbol{F}} & \frac{\partial \boldsymbol{P}}{\partial \boldsymbol{T_c}} \\ \frac{\partial \boldsymbol{Q}}{\partial \boldsymbol{E}} & \frac{\partial \boldsymbol{Q}}{\partial \boldsymbol{F}} & \frac{\partial \boldsymbol{Q}}{\partial \boldsymbol{T_c}} \\ \frac{\partial \boldsymbol{V^2}}{\partial \boldsymbol{E}} & \frac{\partial \boldsymbol{V^2}}{\partial \boldsymbol{F}} & \frac{\partial \boldsymbol{V^2}}{\partial \boldsymbol{T_c}} \\ \frac{\partial \boldsymbol{H}}{\partial \boldsymbol{E}} & \frac{\partial \boldsymbol{H}}{\partial \boldsymbol{F}} & \frac{\partial \boldsymbol{H}}{\partial \boldsymbol{T_c}} \end{bmatrix} \qquad (5)$$

The elements in the Jacobian ($\boldsymbol{J}$) matrix in Equation (5) can be referred to in [10].

The WDPF algorithm is capable of accurately performing weather-dependent PFA. For every iteration of the WDPF power flow execution, accurate conductor temperatures are evaluated based on the heat balance model. Accurate branch resistances are then calculated based on the conductor temperatures (Equation (6)), and the network admittance matrix is updated to execute the next iteration of the weather-dependent power flow. Through this process, accurate power system states and conductor temperatures that reflect the impact of weather are achieved.

$$R(T_c) = \left[\left(\frac{R(T_{\text{high}}) - R(T_{\text{low}})}{T_{\text{high}} - T_{\text{low}}} \right) (T_c - T_{\text{low}}) + R(T_{\text{low}}) \right] \qquad (6)$$

III. Weather-Dependent Multi-Machine Transient Stability Analysis

A precursor to conventional MMTSA is the execution of an initial power flow to evaluate the initial steady-state pre-fault states of the system. To perform a weather-dependent MMTSA, the initial power flow is substituted with the

$$H_{ij}(T_{c_{ij}}) = q_{c_{ij}} + q_{r_{ij}} - q_{s_{ij}} - (E_i^2 + E_j^2 + F_i^2 + F_j^2 - 2E_iE_j - 2F_iF_j)g_{ij} = 0 \qquad (2)$$

WDPF algorithm. This incorporates the impact of weather into MMTSA. TSA is then performed by introducing a fault in the network and performing time-domain simulation of the swing equations. This yields a weather-dependent MMTSA. A methodology for weather-dependent MMTSA is as follows.

Consider a power network with m machines as shown in Figure 1. The generators are connected to the buses in the network with their direct-axis transient reactance X'_d.
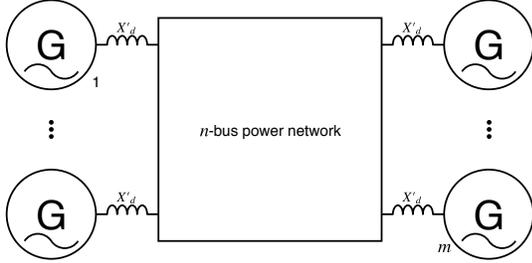

Fig. 1. Multi-machine representation of an n-bus power network.

A WDPF is executed, as a first step, to calculate the weather-dependent power system states for the initial pre-fault steady-state condition. Therefore, WDPF yields the weather-dependent power system states that include voltages of the buses, temperatures of the branches, power injections of the generators, etc.

Given the power injections ($\tilde{S}_k$), the machine currents ($\tilde{I}_k$) are calculated as shown in Equation (7).

$$\tilde{I}_k = \frac{\tilde{S}_k^*}{\tilde{V}_k^*} \quad \text{for } k = 1, \ldots, m \tag{7}$$

The generator voltages ($\tilde{E}'_k$) behind their direct-axis transient reactances (X'_{d_k}) are then calculated using Equation (8).

$$\tilde{E}'_k = \tilde{V}_k + jX'_{d_k}\tilde{I}_k \quad \text{for } k = 1, \ldots, m \tag{8}$$

The electrical power (MW) input (P_{e_k}) by the generators into the network is now calculated by Equation (9).

$$P_{e_k} = \Re\left(\tilde{E}'_k \tilde{I}_k^*\right) \quad \text{for } k = 1, \ldots, m \tag{9}$$

Input losses to the generators are neglected and therefore the electrical power (P_{e_k}) is equal to the mechanical inputs (P_{m_k}) to the generators. All the weather-dependent initial pre-fault steady-state conditions are now available. These include the pre-fault mechanical input powers (P_{m_k}), the pre-fault rotor angles (δ_{0_k}), and the pre-fault generator and bus voltages ($\tilde{E}'_k$ and $\tilde{V}_k$).

Network equations representing the pre-fault, during-fault, and post-fault conditions are then formed to establish the relationship between generator voltages ($\tilde{E}'_k$) and bus voltages ($\tilde{V}_k$) during the aforementioned conditions. Consider the equation of the bus injection current shown in Equation (10) where the admittance matrix (Y_{WDPF}) is weather-dependent.

$$\tilde{\boldsymbol{I}} = \tilde{\boldsymbol{Y}}_{\mathrm{WDPF}}\tilde{\boldsymbol{V}} \tag{10}$$

For the n-bus power network with m machines shown in Figure 1, Equation (10) can be represented as Equation (11).

All the load-bus current injections can be considered 0 by converting all the loads to equivalent admittances ($\tilde{y}_{\mathrm{load}_k}$) as presented in Equation (12) and adding to the weather-dependent admittance matrix ($\tilde{\boldsymbol{Y}}_{\mathrm{WDPF}}$) yielding Equation (13).

$$\begin{bmatrix} \tilde{I}_1 \\ \vdots \\ \tilde{I}_m \\ \vdots \\ \tilde{I}_n \end{bmatrix} = \begin{bmatrix} \tilde{Y}_{11} & \cdots & \tilde{Y}_{1m} & \cdots & \tilde{Y}_{1n} \\ \vdots & \ddots & \vdots & \ddots & \vdots \\ \tilde{Y}_{m1} & \cdots & \tilde{Y}_{mm} & \cdots & \tilde{Y}_{mn} \\ \vdots & \ddots & \vdots & \ddots & \vdots \\ \tilde{Y}_{n1} & \cdots & \tilde{Y}_{nm} & \cdots & \tilde{Y}_{nn} \end{bmatrix} \begin{bmatrix} \tilde{V}_1 \\ \vdots \\ \tilde{V}_m \\ \vdots \\ \tilde{V}_n \end{bmatrix} \tag{11}$$

$$\tilde{y}_{\mathrm{load}_k} = \frac{\tilde{S}_k^*}{|V_k|^2} \quad \text{for } k = 1, \ldots, n \tag{12}$$

$$\begin{bmatrix} \tilde{I}_1 \\ \vdots \\ \tilde{I}_m \\ 0 \\ \vdots \\ 0 \end{bmatrix} = \begin{bmatrix} \left(\tilde{Y}_{11} + \tilde{y}_{\mathrm{load}_1}\right) & \cdots & \cdots & \cdots & \cdots \\ \vdots & \ddots & \vdots & \vdots & \vdots \\ \cdots & \cdots & \left(\tilde{Y}_{mm} + \tilde{y}_{\mathrm{load}_m}\right) & \cdots & \cdots \\ \vdots & \ddots & \vdots & \ddots & \vdots \\ \cdots & \cdots & \cdots & \cdots & \left(\tilde{Y}_{nn} + \tilde{y}_{\mathrm{load}_n}\right) \end{bmatrix} \begin{bmatrix} \tilde{V}_1 \\ \vdots \\ \tilde{V}_m \\ \tilde{V}_{m+1} \\ \vdots \\ \tilde{V}_n \end{bmatrix} \tag{13}$$

In Equation (13), the nonzero current injections ($\tilde{I}_k$) represent the injections from the m machines, which are calculated as shown in Equation (14).

$$\tilde{I}_k = \tilde{y}'_{d_k}\left(\tilde{E}'_k - \tilde{V}_k\right) \quad \text{for } k = 1, \ldots, m \tag{14}$$

In Equation (14), $\tilde{y}'_{d_k} = \frac{1}{jX'_{d_k}}$, i.e. the admittance connecting the generator to the bus in the network. Substituting Equation (14) in Equation (13) and rearranging yields Equation (15).

$$\begin{bmatrix} \tilde{y}'_{d_1}\tilde{E}'_1 \\ \vdots \\ \tilde{y}'_{d_m}\tilde{E}'_m \\ \vdots \\ 0 \end{bmatrix} = \begin{bmatrix} \left(\tilde{Y}_{11} + \tilde{y}_{\mathrm{load}_1} + \tilde{y}'_{d_1}\right) & \cdots & \cdots & \cdots \\ \vdots & \ddots & \vdots & \ddots & \vdots \\ \cdots & \cdots & \left(\tilde{Y}_{mm} + \tilde{y}_{\mathrm{load}_m} + \tilde{y}'_{d_m}\right) & \cdots & \cdots \\ \vdots & \ddots & \vdots & \ddots & \vdots \\ \cdots & \cdots & \cdots & \cdots & \left(\tilde{Y}_{nn} + \tilde{y}_{\mathrm{load}_n}\right) \end{bmatrix} \begin{bmatrix} \tilde{V}_1 \\ \vdots \\ \tilde{V}_m \\ \vdots \\ \tilde{V}_n \end{bmatrix} \tag{15}$$

Equation (15) can be solved for the bus voltages ($\tilde{V}_k$) as presented in Equation (16). The resulting admittance matrix in Equation (16) is the sum of the weather-dependent admittance matrix ($\tilde{\boldsymbol{Y}}_{\mathrm{WDPF}}$), the diagonal load admittance matrix ($\tilde{\boldsymbol{y}}_{\mathrm{load}}$), and the diagonal generator reactance matrix ($\tilde{\boldsymbol{y}}_{\boldsymbol{d}}$).

$$\begin{bmatrix} \tilde{V}_1 \\ \vdots \\ \tilde{V}_m \\ \vdots \\ \tilde{V}_n \end{bmatrix} = \underbrace{\begin{bmatrix} \left(\tilde{Y}_{11} + \tilde{y}_{\mathrm{load}_1} + \tilde{y}'_{d_1}\right) & \cdots & \cdots & \cdots \\ \vdots & \ddots & \vdots & \ddots & \vdots \\ \cdots & \cdots & \left(\tilde{Y}_{mm} + \tilde{y}_{\mathrm{load}_m} + \tilde{y}'_{d_m}\right) & \cdots & \cdots \\ \vdots & \ddots & \vdots & \ddots & \vdots \\ \cdots & \cdots & \cdots & \cdots & \left(\tilde{Y}_{nn} + \tilde{y}_{\mathrm{load}_n}\right) \end{bmatrix}^{-1}}_{\left(\tilde{\boldsymbol{Y}}_{\mathrm{WDPF}} + \tilde{\boldsymbol{y}}_{\mathrm{load}} + \tilde{\boldsymbol{y}}_{\boldsymbol{d}}\right)^{-1}} \begin{bmatrix} \tilde{y}'_{d_1}\tilde{E}'_1 \\ \vdots \\ \tilde{y}'_{d_m}\tilde{E}'_m \\ \vdots \\ 0 \end{bmatrix} \tag{16}$$

The resulting admittance matrix ($\tilde{\boldsymbol{Y}}_{\mathrm{WDPF}} + \tilde{\boldsymbol{y}}_{\mathrm{load}} + \tilde{\boldsymbol{y}}_{\boldsymbol{d}}$) in Equation (16) is an essential element for performing the weather-dependent MMTSA. Equation (16) is solved with the swing equations [1]–[4] of the generators via the process of solving DAE to perform a full weather-dependent MMTSA.

The use of WDPF algorithm and weather-dependent admittance matrix ($\tilde{\boldsymbol{Y}}_{\mathrm{WDPF}}$) to obtain weather-dependent pre-fault, during-fault, and post-fault states, makes this approach more accurate and enables the study of the impact of weather on MMTSA.

IV. CASE STUDY DETAILS

MMTSA is carried out by fault simulation considering the IEEE 30-bus test case which represents a part of the American Electric Power system [17], [18]. The system has 6 generators (including the slack bus) and the remaining buses are load buses (PQ type). The network comprises a total of 41 branches, out of which 34 are weather-dependent, i.e. the other 7 branches are lossless branches. The IEEE 30-bus test network data does not comprise any conductor-specific or weather-specific details [10], [17], [18]. Therefore, for the purpose of the simulation case study, it is assumed that all branches in the 30-bus network are replaced by the 795 kcmil 26/7 Drake ACSR conductor [15] that yields the equivalent network impedance (given in the data).

To study the impact of weather on MMTSA, weather data for the year 2017 was collected from the National Renewable Energy Laboratory's National Solar Radiation Data Base (NSRDB) [19] for Bismarck, North Dakota, USA. The selected location has one of the largest temperature difference between its coldest and hottest day. The coldest (in January) and the hottest (in August) weather data point in 2017 have been selected for the purpose of the simulation. The weather parameters and their values are presented in Table I.

TABLE I
COLDEST AND HOTTEST WEATHER CONDITIONS IN 2017

Weather parameter	Coldest	Hottest
Ambient temperature (°C)	−31	39
Wind speed (m/s)	1.6	5
Wind incidence angle (°)	44.3	20.9
Solar irradiance (W/m^2)	0	699

Three-phase to ground faults were simulated at Bus 2 (which has the highest power generation) in the IEEE 30-bus network to analyse the transient stability by evaluating the critical clearing time (CCT) (t_{cr}). The network was simulated for a total duration of 10 seconds and a simulation time-step of 0.001 seconds was used. The three-phase to ground fault was introduced at 0.5 seconds, which was then cleared after 100 ms at 0.6 seconds. For comparison, the conventional MMTSA was also simulated. The simulation study was conducted in MATLAB®.

V. SIMULATION RESULTS & DISCUSSION

The CCT (t_{cr}) for conventional MMTSA, the coldest and hottest weather conditions, with increasing real load at Bus 2 and Bus 4 is investigated first. The loads at Bus 2 and Bus 4 are increased as Bus 2 is the fault bus, and Bus 4 is the only PQ bus that connects directly to Bus 2. As a result, increasing the load at these two buses would directly impact the MMTSA when fault is introduced at Bus 2. The CCT (t_{cr}) for the aforementioned simulation is presented in Figure 2.

Figure 2 clearly highlights the difference between conventional and weather-dependent MMTSA. As the loading increases by more than 10 times the standard load, the difference between the conventional and weather-dependent CCT (t_{cr}) further increases. Moreover, the CCT (t_{cr}) for all
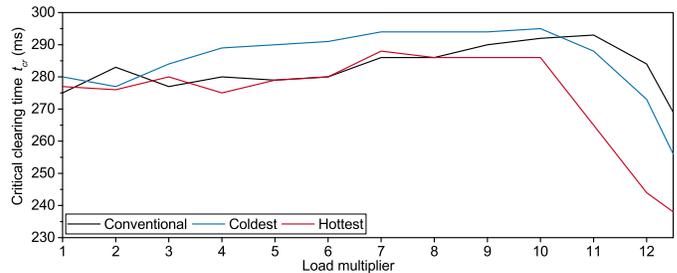

Fig. 2. CCT (t_{cr}) for conventional MMTSA, the coldest and hottest weather conditions, for fault at Bus 2 with increasing real load.

three scenarios (conventional, coldest, and hottest) drastically falls. Both the coldest and hottest weather conditions yield lower CCT (t_{cr}) in comparison to the conventional approach, indicating differences that may lead to power system protection issues if the conventional approach is relied upon. As the load increases from 3 times to 10 times the standard load, the CCT (t_{cr}) for the coldest weather condition is observed to be higher, indicating more accurate transient stability that cannot be evaluated using the conventional approach.

The aforementioned simulation results refer to the IEEE 30-bus as a transmission network. For the purpose of studying the impact of weather on TSA of a distribution network, the IEEE 30-bus network is modified by increasing the R/X ratio to 4 times the standard value. Simulations similar to the previous scenario have been repeated and the results are presented in Figure 3.
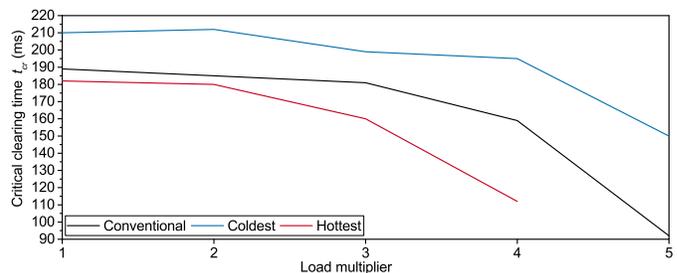

Fig. 3. CCT (t_{cr}) for conventional MMTSA, the coldest and hottest weather conditions, for fault at Bus 2 with increasing real load in IEEE 30-bus network representing a distribution network.

Figure 3 shows a larger difference between the coldest and the hottest weather condition. It is also observed that as the load increases, the difference between these increase further. The coldest weather condition yields a higher CCT (t_{cr}) compared to the conventional and hottest weather condition. This indicates a greater margin of fault clearing time in colder weather conditions. As seen in Figure 3, CCT (t_{cr}) for load increase to 5 times was not evaluated for the hottest weather condition. This is due to divergence of power flow solution for the hottest weather condition indicating potential system instability under such a weather condition. However, the same network with the same loading conditions converges on the coldest weather condition, highlighting the importance of

weather-dependent TSA. Power flow for the network diverges (for conventional and coldest) beyond 5 times load increase.

In order to better understand the impact of weather and increasing R/X ratio on the TSA, further simulations are performed, and the results are presented in Figure 4.
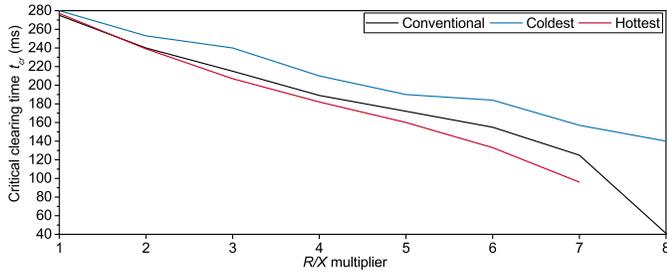

Fig. 4. CCT (t_{cr}) for conventional MMTSA, the coldest and hottest weather conditions, for fault at Bus 2 with increasing R/X ratio.

Figure 4 shows that as the R/X increases to 8 times, the CCT (t_{cr}) reduces while the difference between the coldest and the hottest weather condition increases. This indicates a strong correlation between weather and transient stability of networks with higher R/X ratios such as distribution networks. Similar to the previous results (Figure 3), the power on the hottest weather condition did not converge when R/X ratio was 8 times higher.

A. Results Summary & Discussion

In summary, the above weather-dependent MMTSA simulation case study demonstrates the impact of weather conditions on MMTSA, and highlights the differences and benefits of considering weather conditions in such analyses. It is understood from the investigation that the changing weather conditions affect the stability indicators i.e. the CCT and critical clearing angle causing them to vary with the weather conditions. Therefore, as the weather condition change, the stability indicators are constantly being affected. This indicates potential power system protection issues, e.g. protection devices like circuit breakers may no longer be confidently set based on stability studies neglecting the effect of weather conditions. Furthermore, an impact on the R/X ratio of the network lines due to changing weather conditions impacting MMTSA is also observed. For example, networks with increased R/X ratio such as distribution networks are expected to have greater impact of weather on transient stability, which makes weather considerations important for studying the TSA of distribution systems. In addition, increasing integration of distributed generation in the distribution system leading to lower inertia further threatens transient stability and calls for improved and accurate TSA approaches such as the weather-dependent TSA presented.

In conclusion, a methodology to incorporate fully the effects of weather in MMTSA is demonstrated, which could be significant depending on the type of network and actual weather conditions being experienced. Furthermore, the investigation presented enables the study of transient stability for various networks in various regions around the globe experiencing differing weather conditions.

VI. CONCLUSION

The weather-dependent MMTSA approach demonstrated here presents a framework for conducting accurate MMTSA incorporating readily available and measured weather data. Weather-dependent MMTSA of the IEEE 30-bus network was investigated and demonstrated, which showed the impact of changing weather conditions on MMTSA. As the simulation results show, this impact is non-negligible for an accurate analysis. Future work entails MMTSA of distribution networks with more detailed machine/inverter models under consideration of weather conditions.

REFERENCES

[1] O. Elgerd, *Electric Energy Systems Theory: An Introduction*. Tata McGraw-Hill, 1983.
[2] H. Saadat, *Power System Analysis*. PSA Publishing, 2010.
[3] J. Glover, M. Sarma, and T. Overbye, *Power System Analysis and Design*. Cengage Learning, 2011.
[4] P. Kundur, *Power System Stability and Control*, 1st ed. McGraw-Hill, 1994.
[5] F. Milano, Ed., *Advances in Power System Modelling, Control and Stability Analysis*, ser. Energy Engineering. Institution of Engineering and Technology, 2016.
[6] B. Stott, "Power system dynamic response calculations," *Proceedings of the IEEE*, vol. 67, no. 2, pp. 219–241, Feb 1979.
[7] Charles Ventura, "Most of Puerto Rico still in the dark after power plant fire," https://www.usatoday.com/story/news/2016/09/22/puerto-rico-power-outage-electricity-plant/90823454/, Sep. 2016.
[8] NASA, "Climate Change: Vital Signs of the Planet," https://climate.nasa.gov/effects/, 2019, online; accessed September 2019.
[9] A. Kubis and C. Rehtanz, "Application of a combined electro-thermal overhead line model in power flow and time-domain power system simulations," *IET Generation, Transmission & Distribution*, vol. 11, no. 8, pp. 2041–2049, 2017.
[10] A. Ahmed, F. J. Stevens McFadden, and R. K. Rayudu, "Weather-dependent power flow algorithm for accurate power system analysis under variable weather conditions," *IEEE Transactions on Power Systems*, pp. 1–1, 2019.
[11] A. R. Al-Roomi and M. E. El-Hawary, "Effective weather/frequency-based transmission line models - Part II: Prospective applications," in *Electrical Power and Energy Conference (EPEC), 2017 IEEE*. IEEE, 2017, pp. 1–8.
[12] A. Ahmed, F. S. McFadden, and R. Rayudu, "Transient stability study incorporating weather effects on conductors," in *2018 IEEE Power & Energy Society General Meeting (PESGM)*. IEEE, 2018, pp. 1–5.
[13] A. Ahmed, F. Stevens McFadden, R. Rayudu, and T. Massier, "Weather-dependent transient stability asnalysis of single-machine infinite-bus system," in *2019 54th International Universities Power Engineering Conference (UPEC)*, Sep. 2019, pp. 1–6.
[14] S. Frank, J. Sexauer, and S. Mohagheghi, "Temperature-dependent power flow," *IEEE Transactions on Power Systems*, vol. 28, no. 4, pp. 4007–4018, Nov. 2013.
[15] "IEEE standard for calculating the current-temperature relationship of bare overhead conductors," *IEEE Std 738-2012 (Revision of IEEE Std 738-2006 - Incorporates IEEE Std 738-2012 Cor 1-2013)*, pp. 1–72, Dec. 2013.
[16] L. Powell, *Power System Load Flow Analysis*. McGraw-Hill Education, 2004.
[17] "Power Systems Test Case Archive: 30 Bus Power Flow Test Case," http://www.ee.washington.edu/research/pstca/pf30/pg_tca30bus.htm, 1993.
[18] O. Alsac and B. Stott, "Optimal load flow with steady-state security," *IEEE Transactions on Power Apparatus and Systems*, vol. PAS-93, no. 3, pp. 745–751, May 1974.
[19] National Renewable Energy Laboratory, "The NSRDB Data Viewer," https://maps.nrel.gov/nsrdb-viewer/, 2019, online; accessed September 2019.